Experimental report: SI 1691 (BM02)

Strain in core/shell and buried semiconductor nanowires

Participants : J. Eymery, V. Favre-Nicolin, S. Baudot, F. Andrieu, F. Rieutord
Samples from Lund University.
Local contact : N. Boudet
Round 10/2007

This experiment has been mainly focussed on the dielectric/metallic wrap-gate deposition on InAs NWs (grown by L. Fröberg in Lund University: L. Samuelson's group).
With the very small dimensions used in the recent nanowire devices, the dielectric/metallic wrap-gate technological steps may significantly impact the NW active region, and it is necessary to check the NW integrity during the integration process. Several important structural points may be considered as the strain state and defect density which change the transport properties,[Eymery07] or the shape and thickness inhomogeneity which increase the leakage current or the electrostatic control.
These points have been studied with grazing incidence X-ray techniques at different integration levels of horizontal NWs. The study has been focussed on the InAs system, already used in NW transistors, [Bryllert06] resonant devices and optical emitting materials, and particularly on the HfO_2-dielectric and Cr-gate depositions which gives very good characteristics in vertical wrap-gated transistors. [Thelander08] Grazing Incidence X-ray Diffraction (GIXRD) is used to analyse the NW strain during the process. Longitudinal deformation is obtained by the measurements of Crystal Truncation Rods (CTRs), and in-plane deformation by standard GIXRD. The evolution of the NW initial hexagonal shape is analyzed by Grazing Incidence Small Angle Scattering (GISAXS) after the thin oxide and metallic depositions allowing extracting both the thickness of the core/shell structures and the surface shape smoothening.
The nanowire growth is gold-assisted and takes place in a chemical beam epitaxy (CBE) system using trimethylindium, precracked *tert*-butylarsine, and precracked *tert*-butylphosphine as growth precursors. Prior to growth, size-selected Au aerosol particles are deposited on a $InAs(111)_B$ substrate and the sample is deoxidized in the growth chamber at 520 °C under As pressure. The NW density is determined by the Au particle number to about 0.55 ± 0.02 NW/μm^2. As shown in Fig. 1, the NW growths of the InAs NW reference and of the other core/shell heterostructures are well oriented and the narrow orientation distribution allows studying the NW epitaxy according to the substrate lattice. [Eymery07] We use the (*hkl*) Miller indexes corresponding to the InAs $(111)_B$ surface unit cell with hexagonal surface unit cell vectors $\mathbf{a}_1 = 1/2[-110]$, $\mathbf{a}_2 = 1/2[0\text{-}11]$ and $\mathbf{a}_3 = [111]$. Within this basis, InAs $(111)_B$ bulk Bragg reflections are found at $l = 1, 4, 7, \ldots$ for $(h,k) = (1,0)$ and at $l = 2, 5, 8, \ldots$ for $(h,k) = (0,1)$. X-ray experiments were performed under helium flow to prevent sample degradation and air diffuse scattering. Data were collected on the D2AM (and BM32) beamlines using 9.561 keV photon energy. At this energy, the InAs critical angle of total reflection is about 0.3°. For grazing incidence geometry, the beam footprint on the sample surface integrates the intensities of a large number of NWs. Fig. 2 shows the (0 -1 *l*) CTR measurements of the four samples of Fig. 1 for two grazing incidence angles α=0.05° and 0.4° respectively below and above the critical angles of total reflection.

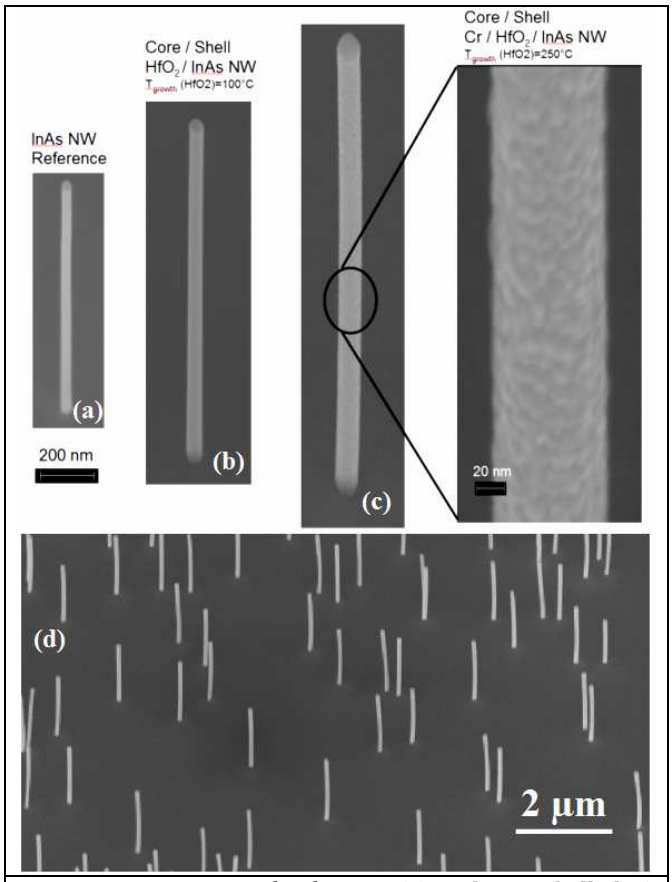

Fig. 1. SEM images of reference (a) and core/shell (b,c) InAs nanowires (NW) grown by chemical beam epitaxy. (b) corresponds to HfO_2-shell grown on a sample similar to reference (a) at 100°C, and (c) to a Cr-shell grown on HfO_2 / InAs (oxide growth is performed at 250°C). (d) shows a tilted-view of the Cr / HfO_2 / InAs core-shell NW assembly. This stacking is representative of the dielectric/metallic wrap-gate used in vertical NW transistors. Note that the tilt angles of the images are different: the diameters may be deduced from the scale bar.

As already explained in a paper dedicated to longitudinal heterostructures, Eymery07 CTR measurements allows the separation of the nanowire contribution from the substrate (S) and overgrowth (TW) signals. The peaks of Fig. 1 can be indexed in three sets in agreement with Ref. Eymery07 and with complementary measurements of the (0 -2 *l*) CTRs, and also at α=0.2° where multiple beam scattering effects can be observed. Zinc-Blende (ZB) peaks at *l*=1, 4 refers to substrate (noted S). They are very weak at small grazing incidence and more intense at larger incidence. Twinned ZB at *l*=2, 5 (noted TW) corresponds to substrate overgrowth and follows the same behaviour as a function of α. The nanowire scattering (NW) is measured at *l*=1.5, 3, 4.5 and corresponds to the wurtzite structure. The intensity doesn't depend strongly on α and NW signal is clearly observed in the transmission regime (α=0.05°). The reference and core/shell structures have the same behaviour, the most streaking feature being the CTR broadening for the Cr-deposited sample. As shown in Fig. 2(c) (for α=0.4° and *l* =4), the positions of the substrate peaks are nearly insensitive to α and to the dielectric and metallic deposition. It gives an internal reference of the lattice distance (and deformation), and allows to check the goniometer alignment. The error bar on the S-peak position measurements is estimated to ±0.065% considering three grazing incidences (0.05°, 0.2°, 0.4°), two CTRs ((0 -1 *l*) , (0 -2 *l*)), and four *l*-values (1, 2, 4, 5). Due to the difference of stacking of the close packed planes between ZB and WZ structure which can be observed along the (0 -1 *l*) CTR, NW and other contributions (S and TW) are well separated in reciprocal space. The NW deformation along *l* (*i.e.* the growth direction) can be measured directly from the $\Delta l/l$ variation between the reference and the core/shell structures. As shown in Fig. 2(c) corresponding to α=0.4° and *l* =4.5, the NW peaks exhibit small shifts for HfO_2-coated NW and larger for Cr-coated-one. These shifts have been carefully measured considering the three grazing incidences, the two CTRs, and the three *l*-values (1.5, 3, 4.5). The *contractions* of the core/shell NWs along the growth direction are 0.95 % ±0.07 for Cr/HfO_2 (T=250°C)/InAs and 0.13 % ±0.07 for HfO_2/InAs grown at 250°C. Similar treatments have been performed for the growth temperature deposition of 100°C for HfO_2 and exhibit a contraction of about 0.26 %.

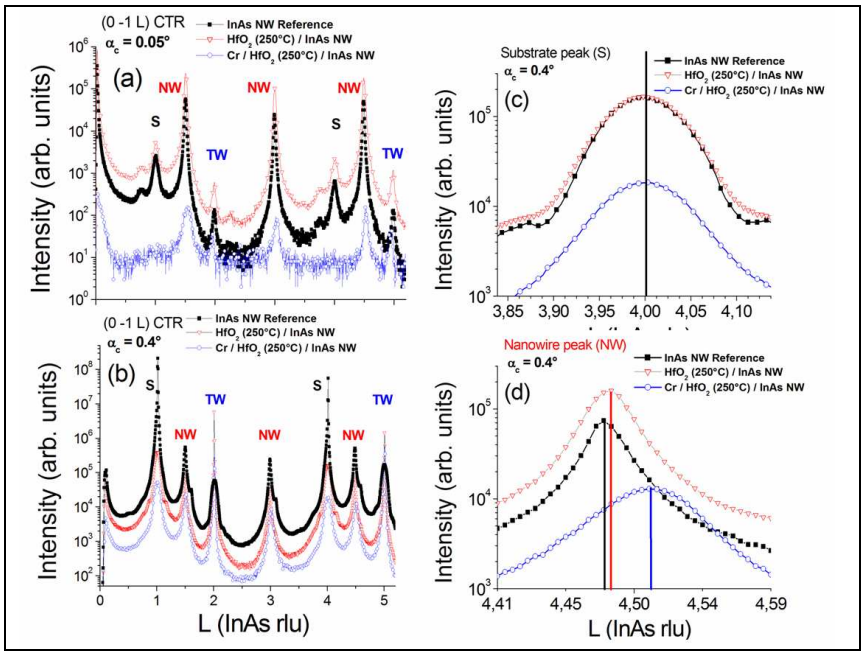

Fig. 2. (0 -1 l) Crystal Truncation Rod (CTR) measurements of reference and core/shell NWs shown in Fig. 1 for two grazing incidences (a) α=0.05° and (b) 0.4°. l is in reciprocal lattice units (rlu) of the cubic InAs(111) substrate (marked by S). Magnifications of (c) the substrate peaks at l = 4 and of (d) the NW peak at l = 4.5.

After having analyzed the growth-axis deformation with X-ray diffraction, we can also access to the average NW shape and size of this assembly with small-angle X-ray scattering (SAXS) at very grazing incidence and emergence ($\alpha = \beta = 0.27°$). Fig. 3 shows selected intensity measurements $I(\psi)$ as a function of the in-plane scattering angle ψ for several sample orientations (azimuth) around the surface normal. Contrary to what is measured for cylindrical cross sections, we observe the dependence on the azimuth ξ of the oscillation fringes due to the NW size in a direction perpendicular to the beam both in position and intensity. The origin $\xi = 0$ is defined by a direction perpendicular to the NW facets. The systematic measurement of $I(\psi)$ as a function of ξ (over $\pi/2$, every $\pi/36$) has shown a $\pi/6$ symmetry. The main features of the azimuth-angle dependence consist of the damping and the shift of the second-order fringe from $\xi = 0$ to $\pi/6$ and of the disappearance of the third oscillation at $\xi = \pi/6$. The centre part of the experimental curve comes from the surface and overgrowth scattering. Note that in this sample, the NW density is very low, so that synchrotron radiation is necessary. From the analysis of the oscillation fringes, it is quite straightforward to deduce the diameter of the InAs reference, but also the thickness of the oxide coating (measurements with oxide deposition at 100°C can also be compared to these results). The Cr coating gives more complicated fringes that must be fitted to extract the shell thicknesses. This quantitative work is presently under way, and the smoothening of the initial hexagonal shape may be estimated.
Complementary experiments with the X-ray reflectivity technique allow estimating the 2D growth of oxide and metal on the flat surface, so that planar and radial growth rates can be given.

To conclude, we show that grazing incidence X-ray diffraction (GIXRD) can be used to measure the strain state along the NW at the different integration steps of the device. Complementary in-plane measurements have been also performed, but their analysis is more difficult due to very strong heterogeneity of the strain field due to the core/shell structure. It is shown that the Cr metallic coating significantly contract the NW, whereas the oxide deposition has a smaller impact. This level of deformation is now studied to understand what the deformation impact on the transport properties is in the InAs system. Small angle scattering has been used to obtain precise information about the core/shell geometry with the thicknesses and shapes evolutions during the process.

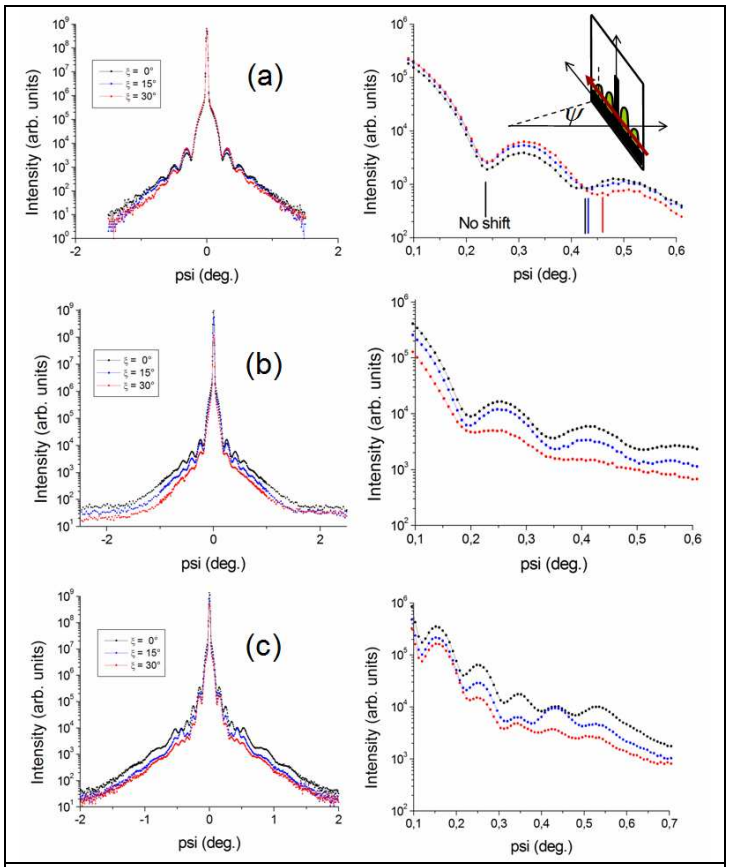

Fig. 3. GISAXS profiles (for incidence and emergence equal to 0.27°) for the NW samples shown in Fig. 1 for several incoming beam orientations ($\xi = 0$ is parallel to the facets of the hexagon-shape NW). (a) uncoated InAs NW, (b) (resp. (c)) HfO_2-shell grown on sample similar to reference (a) at 250°C, and (d) to a Cr-shell grown on sample similar to (c). The right curves give details of the intensity oscillations.

References

J. Eymery, F. Rieutord, V. Favre-Nicolin, O. Robach, Y.M. Niquet, L. Fröberg, T. Mårtensson, L. Samuelson, NanoLetters **7**, 2596 (2007).

T. Bryllert, L.-E. Wernersson, T. Löwgren, and L. Samuelson, Nanotechnology **17**, s277 (2006).

C. Thelander, L. Fröberg, C. Rehnstedt, L. Samuelson, and L.-E. Wernersson, IEEE Electron Device Letters **29**, 206 (2008).